

CrossMark  
click for updatesCite this: *J. Mater. Chem. A*, 2017, 5, 6455

# Electron trapping induced electrostatic adsorption of cations: a general factor leading to photoactivity decay of nanostructured TiO<sub>2</sub>†

Tao He,<sup>\*a</sup> Libo Wang,<sup>a</sup> Francisco Fabregat-Santiago,<sup>\*b</sup> Guoqun Liu,<sup>\*c</sup> Ying Li,<sup>a</sup> Chong Wang<sup>d</sup> and Rengui Guan<sup>a</sup>

In this work, a mechanism of electron trapping induced electrostatic adsorption of electrolyte cations (ETIEA) is proposed to explain the general photoactivity decay of nanostructured TiO<sub>2</sub> electrodes, usually occurring during the initial several minutes of photoelectrochemical (PEC) processes. A series of designed "electron trapping" experiments and combined photo/electrochemical measurements revealed that it is the defect states of TiO<sub>2</sub> that lead to ETIEA. A higher amount of surface defects will lead to larger ETIEA, which consequently accelerates the photoactivity decay. Different from the well-known "trap-filling" effect that decreases transport resistance, we find that the electron-trapping induced electrostatic attraction cannot make trap states inactive but can increase the detrapping energy barrier of trapped electrons. Our research reveals an important but easily overlooked fact, that is, carrier kinetics in nanostructured TiO<sub>2</sub> may not be able to reach a steady state. In other words, a stable photocurrent may not be obtained because the photoelectrochemical process will alter the carrier dynamics constantly due to the existence of defect states. This result could also be applicable to other photoactive semiconductors.

Received 6th February 2017  
Accepted 20th February 2017

DOI: 10.1039/c7ta01132f

rsc.li/materials-a

## 1. Introduction

Nanostructured TiO<sub>2</sub> is an important photoactive semiconductor and widely used in photoelectrochemical (PEC) applications including photovoltaic cells,<sup>1</sup> organic pollutant degradation,<sup>2–5</sup> water splitting,<sup>6–8</sup> and biosensors.<sup>9,10</sup> These promising applications rest not only on its excellent photoelectric properties and exceptionally large specific surface area, but also on its high photochemical stability which is usually the first requirement for realistic applications. In fact, TiO<sub>2</sub> is one of the known photoactive semiconductors showing the highest stability against photochemical corrosion.

However, TiO<sub>2</sub> also exhibits photoactivity decay in some PEC processes. For example, continuous photocurrent attenuation occurs usually during the first several minutes of the chronoamperometric (*i*-*t*) test in PEC degradation of organic pollutants<sup>11,12</sup> and water splitting.<sup>13,14</sup> This kind of photoactivity decay is

generally assigned to the continuous increase of recombination.<sup>11,15</sup> Two factors are considered to be related to the recombination, one is the trapping of photo-generated carriers in intra-band gap states and the other is the accumulation of the formed oxidizing active species at the semiconductor/electrolyte interface.<sup>11–13,15</sup> However, a clear explanation is necessary to further understand the photoactivity decay mechanism.

To date, it is known that surface defect states can exert heavy influence on both the thermodynamics and kinetics of PEC processes.<sup>16–20</sup> They may cause Fermi level pinning or partial pinning in some nanostructured photoelectrodes,<sup>16</sup> which is responsible for the increase of the overpotential for PEC water oxidation.<sup>17,18</sup> They may also act as recombination sites<sup>19</sup> or active sites for hole interface transfer (water oxidation) reactions.<sup>20</sup> Due to the large density of defect states (DODS),<sup>21–23</sup> electron transport in nanostructured semiconductors follows the "trapping–detrapping" mode, usually 10<sup>3</sup> to 10<sup>5</sup> times slower than that in a single crystal.<sup>24,25</sup>

Traps can be filled permanently if a high negative bias is applied to enable protons or Li<sup>+</sup> to insert into the semiconductor lattice. As a result, the electron transport resistance will be remarkably decreased. Such a "trap-filling" effect is widely used to improve the activity of photoactive semiconductors.<sup>26–32</sup> However, electron trapping is still inevitable if the "trap-filling" effect cannot be obtained. For example in n-type TiO<sub>2</sub>, the interface transfer of photogenerated holes

<sup>a</sup>College of Chemistry and Chemical Engineering, Yantai University, China. E-mail: htzyhcy@gmail.com

<sup>b</sup>Photovoltaic and Optoelectronic Devices Group, Institute of Advanced Materials, Universitat Jaume I, 12006 Castelló, Spain. E-mail: fabresan@uji.es

<sup>c</sup>School of Materials and Chemical Engineering, Zhongyuan University of Technology, China. E-mail: flyskylugg@126.com

<sup>d</sup>College of Optoelectronic Information Science and Technology, Yantai University, China

† Electronic supplementary information (ESI) available. See DOI: 10.1039/c7ta01132f

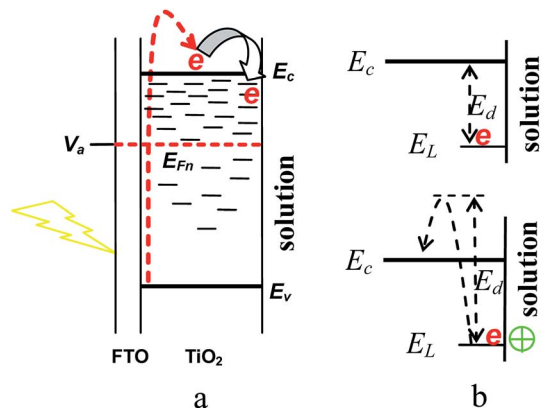


Fig. 1 Schematic diagrams, (a) photogenerated electron trapping in band gap states. The red dashed arrow represents irradiation-induced excitation of electrons into the conduction band and the thick arrow demonstrates electrons being trapped at localized band gap states; (b) the energy barrier ( $E_d$ ) needed for trapped electrons to detrapp to conduction band states (up) and the increase of the  $E_d$  due to electrostatic interactions between trapped electrons and adsorbed cations (down).  $\oplus$  represents cations in electrolyte solution.  $V_a$ ,  $E_{Fn}$ ,  $E_c$ , and  $E_v$  are respectively the applied potential, electron Fermi level, and the energy levels of the conduction band bottom and valence band (top).

occurs in the ns scale while electron transport occurs in the  $\mu$ s or even ms scale,<sup>33</sup> which leads to electron trapping (Fig. 1a).

Herein, we demonstrated another effect, as described below, of surface defect states on the dynamics of electrons in the  $\text{TiO}_2$  electrode which leads to the general photoactivity decay. Within the framework of the multiple trapping model, the energy barrier ( $E_d$ ) for the trapped electrons to detrapp to extended states determines the transport properties of electrons in nanostructured semiconductors.<sup>24,25,34,35</sup> Theoretically,  $E_d$  is equal to  $E_c - E_L$  where  $E_c$  is the lower conduction band edge energy and  $E_L$  is the energy of the localized state in the band gap (Fig. 1b up).<sup>34</sup> However, it is proposed herein that the electrostatic attraction between trapped electrons and counter ions from the electrolyte (protons and other cations) will increase the detrapping energy barrier  $E_d$  (Fig. 1b down), which may be the reason for the general photoactivity decay of the  $\text{TiO}_2$  photoanodes.

The generality of photoactivity decay was demonstrated through static photocurrent measurements using  $\text{TiO}_2$  electrodes quite different in phase structure, primary particle size and shape, and pore structure, and also in various electrolyte systems. A series of combined photo/electrochemical measurements revealed that the electron transport properties decay continuously along with the proceeding of PEC water splitting. Electron trapping/cation adsorption experiments were carried out using  $\text{TiO}_2$  films with a significant difference in the amount of surface defects, giving evidence of the ETIEA-induced photoactivity decay.

## 2. Experimental section

### 2.1 Preparation and characterization of two types of nanostructured $\text{TiO}_2$ films

Single crystal rutile  $\text{TiO}_2$  nanorod arrays were grown hydrothermally on the conducting surface of FTO substrates (the film is designated as R- $\text{TiO}_2$ ).<sup>36</sup> Nanoparticulate  $\text{TiO}_2$ /FTO films were

prepared through the “doctor blade” processing and sintering procedures, and anatase  $\text{TiO}_2$  nanoparticles were prepared using a dialysis procedure<sup>14</sup> (the film is designated as D- $\text{TiO}_2$ ). X-ray diffraction (XRD, Shimadzu-6100 diffractometer with a  $\text{Cu K}\alpha$  radiation source) and scanning electron microscopy (SEM, HITACHI S-4800 FE-SEM) techniques were applied to obtain structural and morphological characteristics of the films.

### 2.2 Electron trapping experiments

All the electrochemical and photoelectrochemical experiments were carried out by using a CHI electrochemical analyzer (CHI660E) with a standard three-electrode system.  $1 \text{ cm}^2$   $\text{TiO}_2$  films were used as the working electrodes; the mass of  $\text{TiO}_2$  in the hydrothermally grown R- $\text{TiO}_2$  film was  $0.0030 \pm 0.0002 \text{ g cm}^{-2}$  and the mass of all the doctor-blade  $\text{TiO}_2$  films was also kept at the same value as that of the R- $\text{TiO}_2$  film; a probe of Ag/AgCl, KCl saturated (218; Shanghai Leici Inc.), placed 5 mm away from the surface of the  $\text{TiO}_2$  film, was used as the reference electrode; a  $2 \text{ cm}^2$  Pt sheet was used as the counter electrode.  $1.0 \text{ M KNO}_3$  solution was used as the electrolyte unless otherwise stated. All of the potential values given herein are referenced to the Ag/AgCl electrode. “Electron trapping” experiments were carried out by applying a negative bias ( $-0.6$  to  $-0.9 \text{ V}$ ) to the  $\text{TiO}_2$  films and keeping this potential for a certain period of time (0–800 s). The  $\text{KNO}_3$  solution in the PEC cell was bubbled with  $\text{N}_2$  continuously to eliminate  $\text{O}_2$  during the whole experiments.

In order to verify “electron trapping” induced electrostatic adsorption of electrolyte cations, three separate experiments were designed.

The first experiment was carried out under dark and anaerobic conditions.  $10 \text{ mg L}^{-1}$  cationic dye methylene blue (MB) solution was used as the electrolyte. After reaching adsorption equilibrium under open circuit conditions, a  $-0.8 \text{ V}$  bias was applied to the  $\text{TiO}_2$  film until another adsorption equilibrium is established. Then, the bias was shifted to  $0.8 \text{ V}$ . During the experiment, we tracked the MB concentration by measuring the absorbance of the solution with a UV-visible spectrophotometer (Shanghai METASH UV-6000PC).

For the second one, 3 drops of a solution of phenolphthalein dissolved in ethanol (0.5 wt%) were added into the  $1 \text{ M KNO}_3$  electrolyte beforehand, and the color change of the  $\text{TiO}_2$  electrode was recorded during the “electron trapping” process.

In the last one, phosphate-modified  $\text{TiO}_2$  nanoparticulate electrodes<sup>37</sup> were used. The  $\text{TiO}_2$  powder was scraped out of the film before and after the “electron trapping” experiment; IR spectra were measured with Fourier transform infrared spectroscopy (Shimadzu IRAffinity-1) and the KBr-tablet technique.

### 2.3 Photo/electrochemical measurements

Chronoamperometric measurements ( $i-t$ ) under super band gap irradiation were carried out by using a  $365 \text{ nm}$  LED lamp (LHFC084-10,  $0.6 \text{ W cm}^{-2}$ , Shenzhen Lamplic Science Co., Ltd.) connected to a controller (UVEC-4II, Shenzhen Lamplic Science Co., Ltd.). All the  $\text{TiO}_2$  films were irradiated from the backside; the distance between the film and LED was kept constant at  $0.8 \text{ cm}$ .

In order to explore the mechanism of the continuous photocurrent decay, a series of combined photoelectrochemical measurement schemes were designed. The main idea is to track the time-dependent evolution of the photoactivity-determining parameters along with the proceeding of the PEC process. For example, impedance measurements (EIS) in the dark were carried out immediately after a certain period of the  $i-t$  process (100–800 s). This allowed us to investigate the evolution of electron transport properties during the PEC water splitting process. The combined measurements including  $i-t$ /EIS,  $i-t$ /CV and  $i-t$ /M-S are controlled automatically with macro command programs (CHI 660e), and there is no time interval between them.

### 3. Results and discussion

#### 3.1 General and continuous photoactivity decay of nanostructured TiO<sub>2</sub>

Fig. 2 shows that all the  $i-t$  curves feature a photocurrent spike at the beginning of UV light irradiation. These spikes are very common and result from photogenerated electrons being trapped in intra-band gap states (and other capacitive contributions such as Helmholtz capacitance). Following this spike there is continuous and obvious photocurrent attenuation which proceeds at least for 500 seconds (please check Fig. S1† for R-TiO<sub>2</sub> for clearer viewing). The LED light source is checked with a UV sensor, precluding attenuation of UV light intensity. Therefore, the continuous drop of the photocurrent after the spikes is indicative of the photoactivity decay of the photoelectrodes. Compared to D-TiO<sub>2</sub>, the R-TiO<sub>2</sub> film shows a much higher photocurrent and much slower decay (Fig. 2a and b). With the photocurrent at 100 s as the initial value, the decays at 500 s are respectively 7.7% for R-TiO<sub>2</sub> and 16.9% for the D-TiO<sub>2</sub> film. Recently, the photocurrent decays of Cu<sub>2</sub>O, Cu<sub>2</sub>O/CuO and CuO nanorod films have been reported.<sup>38</sup> After a 15 minute chopped light  $i-t$  process where the irradiation duration is also *ca.* 500 s, the decay rates are respectively 15%, 33% and 2%. It can be seen that the TiO<sub>2</sub> films used herein do not show obvious superiority in stability although Cu<sub>2</sub>O is known for suffering photoelectrochemical corrosion.<sup>39–42</sup>

The  $i-t$  measurements were also carried out with other TiO<sub>2</sub> films (Fig. S2, Table S1†) or in different electrolytes, all

exhibiting continuous photocurrent attenuation (Fig. S3†). These facts indicate that the photoactivity decay is, in general, not related to the film structure, morphology, the kind and concentration of electrolyte, or if hole scavengers exist or not.

#### 3.2 The nanostructures, electrochemically active surface area (EASA) and defect states of three TiO<sub>2</sub> films

For nanostructured semiconductors, the film structure/morphology and the distribution of band gap trap states exert great influence on carrier dynamics including transport, interface charge transfer and recombination.<sup>15,22,43</sup> Herein, three typical TiO<sub>2</sub> films including R-TiO<sub>2</sub>, D-TiO<sub>2</sub> and D-TiO<sub>2</sub>-9 h (obtained by heating the D-TiO<sub>2</sub> film at 550 °C in an air atmosphere for 9 hours) are comparatively investigated. The hydrothermally grown R-TiO<sub>2</sub> film is composed of an array of rutile TiO<sub>2</sub> single crystal rods with a diameter of *ca.* 250 nm and the axial [001] direction perpendicular to the FTO surface (Fig. 3a and S2i and j, S1†). Both D-TiO<sub>2</sub> and D-TiO<sub>2</sub>-9 h are constructed with randomly aggregated anatase TiO<sub>2</sub> nanoparticles with a size of *ca.* 16 nm (Table S1†), leading to the formation of nanopores dispersed within the film (Fig. 3b). Meanwhile, XRD and SEM characterizations indicate that the 9 hour heating at 550 °C changes little the film structure and morphology (Fig. S2e–h and Table S1†).

The EASA is usually considered as one of the performance-determining parameters for electrode films. It is known that the EASA of electrodes shows a linear relationship with their geometric double layer capacitance ( $C_{dl}$ ).<sup>44,45</sup> A series of cyclic

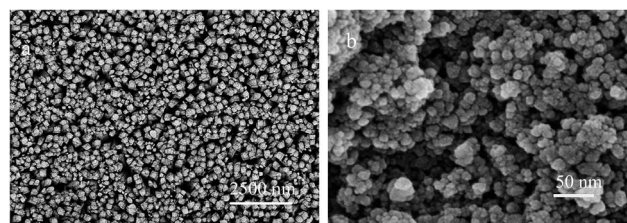


Fig. 3 SEM images of R-TiO<sub>2</sub> (a) and D-TiO<sub>2</sub> (b) films. The TiO<sub>2</sub> mass in the R-TiO<sub>2</sub> film is weighed to be  $0.0030 \pm 0.0002$  g cm<sup>-2</sup>, and the TiO<sub>2</sub> mass in all other doctor-blade TiO<sub>2</sub> films is also kept to be this value.

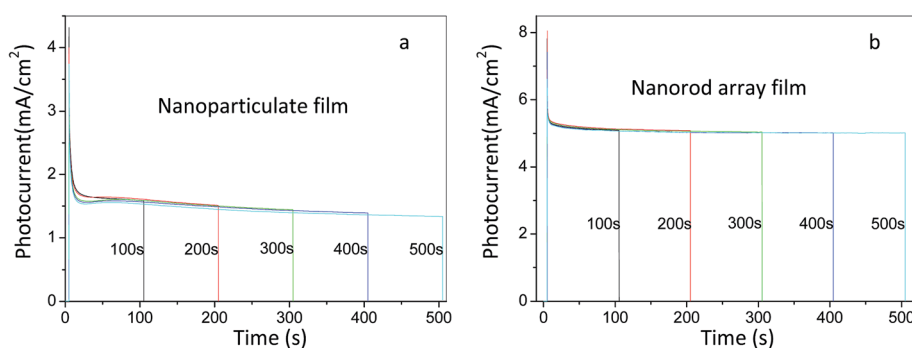


Fig. 2  $i-t$  curves of (a) D-TiO<sub>2</sub> and (b) R-TiO<sub>2</sub> electrodes measured under continuous UV irradiation for five different periods of time. The electrolyte is 1.0 M KNO<sub>3</sub>, and the potential bias is +0.6 V vs. Ag/AgCl.

voltammetry measurements at different CV scan rates are carried out in a non-faradaic potential region. A linear trend is observed when plotting the difference in current density ( $J$ ) between the anodic and cathodic sweeps (*i.e.*  $J_{\text{anodic}} - J_{\text{cathodic}}$ ) at a set potential against the CV scan rate. These data are then fit to a line, the slope of which is equal to twice the geometric  $C_{\text{dl}}$ . Thus, the  $C_{\text{dl}}$  measurements provide a method to estimate and compare the EASA of different electrode films.<sup>44,45</sup>

The inset in Fig. 4a shows the extracted  $C_{\text{dl}}$  values which are comparable to those of some other nanostructured films.<sup>44,45</sup> Assuming the EASA of FTO to be  $1 \text{ cm}^2$ , that is, assuming the conducting surface of the FTO to be totally flat, the estimated EASA of R-TiO<sub>2</sub>, D-TiO<sub>2</sub> and D-TiO<sub>2</sub>-9 h films is respectively 4.99, 76.0 and  $74.67 \text{ cm}^2$  per  $1 \text{ cm}^2$  geometric surface area, giving roughness factors of 4.99, 76.0 and 74.67 for the above three films. We note that these values are several to ten-fold smaller than those derived from other methods for the TiO<sub>2</sub> films with a similar structure and morphology.<sup>47–49</sup> For example, the reported values are 35.22 for the rutile TiO<sub>2</sub> nanorod array<sup>47</sup> and 96–780 for nanoparticulate films.<sup>48,49</sup> One of the reasons leading to this discrepancy may come from the underestimated EASA of FTO since the conducting surface of FTO does also show some roughness (Fig. s5†). Fig. 4a indicates that the EASA of the R-TiO<sub>2</sub> film is 15 times smaller than that of the other two nanoparticulate films, which is probably due to the much larger particle size of the nanorods and the same TiO<sub>2</sub> mass among the three films. For the two nanoparticulate films, on the other hand, the 9 hour heating process at  $550 \text{ }^\circ\text{C}$  causes the EASA to reduce by only 1.75%, consistent with the XRD and SEM results showing that the two films have quite the same structure and morphology (Fig. s2e–h†). The values of the  $C_{\text{dl}}$  and EASA of all the films used in this work are given in Table S1.†

The energy distribution of band gap trap states can be mapped with electrochemical methods such as cyclic voltammetry,<sup>22,23,50</sup> impedance,<sup>34,51</sup> temperature-dependent admittance,<sup>43</sup> temperature-dependent capacitance–frequency and dark current–voltage<sup>52</sup> measurements. Fig. 4b shows the first cycle of their CV curves measured under anaerobic conditions. The current response in the non-faradaic domain ( $-0.2$  to  $-0.85 \text{ V}$ ) comes mainly from electron trapping in band gap

defect states or in conduction band states.<sup>22,23,50</sup> In the potential range below the conduction band edge ( $-0.741 \text{ V vs. Ag/AgCl}$ ) (Fig. 4b), the current increases exponentially, consistent with the exponential distribution of band gap defect states.<sup>22,23,50</sup> For nanostructured semiconductors, the location of the defect states is considered to be mainly surface-related, that is, at the surface and/or grain boundary.<sup>22,53–55</sup> Therefore, the CV measurements provide ways for mapping the distribution of surface defect states in TiO<sub>2</sub> band gaps.<sup>22,23,56</sup>

Several points can be drawn from Fig. 4b. Firstly, although the density of defect states (DODS) of the three films (calculated by dividing the current by  $\text{EASA} \times \text{scanning rate}$ ) is comparable (Fig. s6†), the surface defect state chemical capacitance (indicative of the total amount of surface defect states) of the R-TiO<sub>2</sub> film (calculated by dividing the current by the scanning rate) is far lower than that of the other two films. It is understandable that the R-TiO<sub>2</sub> film has the smallest EASA (Fig. 4a). Secondly, monoenergetic trap states<sup>22,56,57</sup> can be detected in the CV curves of the two nanoparticulate films (centered at  $-0.336 \text{ V}$  for D-TiO<sub>2</sub> and at  $-0.451 \text{ V}$  for D-TiO<sub>2</sub>-9 h) but not in the nanorod array films. It has been revealed that the location of this type of trap state is probably at grain boundaries.<sup>22,56</sup> The R-TiO<sub>2</sub> film is constructed with isolated single crystal nanorods and has no grain boundary. Thirdly, for D-TiO<sub>2</sub> and D-TiO<sub>2</sub>-9 h, the 9 hour heat treatment is an effective way to reduce surface defects in spite of changing little their EASA (Fig. 4a). Finally, it should be noted that the heat treatment moves the monoenergetic trap states towards a higher energy level by 115 mV, for which the reason is not clear.

### 3.3 Possible reasons for the general photoactivity decay

The photoelectrochemical corrosion which is common for other non-TiO<sub>2</sub> semiconductors such as Cu<sub>2</sub>O,<sup>39–42</sup> ZnO<sup>42</sup> and CdS<sup>42,58</sup> can lead to irreversible photoactivity decay. The  $i$ - $t$  curves from multiple measurements can nearly coincide with each other (Fig. 2a and b), excluding this possibility. Other possible reasons leading to the photoactivity decay such as electron acceptors (O<sub>2</sub> and other oxidation products) accumulating in the pores of the film and Fermi level pinning have also been ruled out with experimental evidence (S2†).

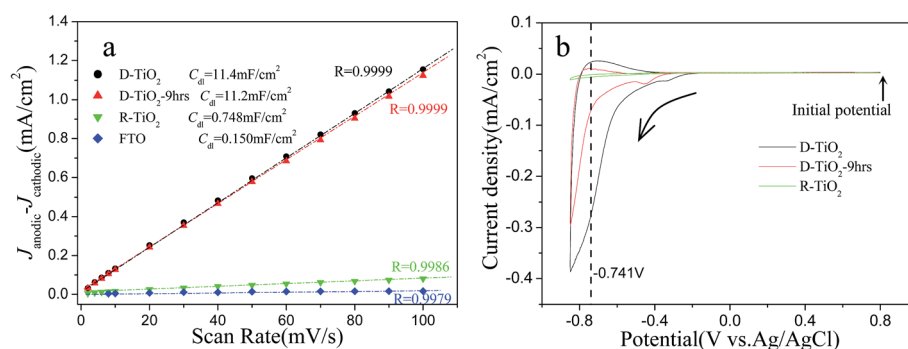


Fig. 4 (a) Dependence of  $J_{\text{anodic}} - J_{\text{cathodic}}$  on CV scan rates to extract  $C_{\text{dl}}$  for FTO and the three TiO<sub>2</sub> films. The measurements in detail are given in Fig. s4.† (b) The first cycle of the CV measurements under anaerobic conditions; the scan rate is  $0.005 \text{ V s}^{-1}$ . The films are pre-immersed in electrolyte for 30 minutes to reach a static equilibrium. The arrow inset in (b) indicates the potential scan direction; the dashed line marks the position of the conduction band edge level calculated with the equation  $E_{\text{CB}} \text{ (vs. Ag/AgCl)} = -0.13 + 0.059\text{pH} - 0.198$ .<sup>46</sup>

The stark differences in the film structure/morphology and distribution of trap states may be used to explain why the R-TiO<sub>2</sub> film gives a higher photocurrent than that of the other two nanoparticulate films. Firstly, the single crystal nature and no grain boundaries of the rutile TiO<sub>2</sub> rods guarantee much faster charge transport in the R-TiO<sub>2</sub> film.<sup>36,59,60</sup> Secondly, as far as defects are concerned, the bulk defects are usually regarded as recombination sites,<sup>61,62</sup> while the role of surface-related defects may be quite different in different systems. During the photocatalytic degradation of organic compounds with both rutile and anatase TiO<sub>2</sub> nanoparticles, the surface defects, usually oxygen vacancies, can promote the separation of electron–holes pairs under irradiation, and therefore, enhance photoactivity.<sup>62</sup> However, in PEC systems the surface-related defects<sup>22,53–55</sup> especially the grain boundary defects (deep monoenergetic trap sites)<sup>22,56,57</sup> are usually regarded as recombination sites. The R-TiO<sub>2</sub> has the least amount of surface defects and has no monoenergetic trap sites, implying that the recombination might also be minimal. The heat treatment at 550 °C for 9 h gives further evidence. Both D-TiO<sub>2</sub> and D-TiO<sub>2</sub>-9 h are quite close in the film structure/morphology and EASA (they are actually the same one film); the latter has fewer surface defects and a much higher photocurrent.

Nevertheless, the continuous photocurrent decay and the quite different decay rates among the three films can still be a mystery if focusing only on the above factors. Along with the proceeding of the PEC process, there should be some aspect which is in a state of dynamic changing and consequently leads to this continuous decay.

The surface-related defect states include exponential band tails<sup>22,23,53,56,57</sup> and monoenergetic deep trap states.<sup>22,56,57</sup> They make electron transport behavior distinct from that in single crystals. When the electron Fermi level is lower than the conduction band edge, traps exert influence on electron transport by “multiple trapping”<sup>24,25,34,35</sup> and/or “hopping”<sup>63,64</sup> modes. Considering various physical/chemical processes occurring at the semiconductor/electrolyte interface, the surface-related trap states may not be always in the static state. For example, covalent bonding between protons and O–Ti<sup>65</sup> and proton intercalation<sup>66</sup> can give some new trap states with higher barriers for

the diffusion of carriers. This implies that the electron transport behavior may not be always in the static state either.

Recently, the interaction between accumulated electrons inside TiO<sub>2</sub> and cations in the surrounding electrolyte has been studied with the Stark effects of an organic dye, LEG4, as the probes.<sup>67</sup> The authors proposed that electroadsorbed cations act as electrostatic trap states for electrons in the mesoporous TiO<sub>2</sub> electrode. Actually, this kind of interaction has been paid attention long time ago.<sup>68</sup> While, the mechanism of the interaction and its influence on the photoelectron properties of TiO<sub>2</sub> are still poorly understood.

Herein, it is proposed, as depicted in Fig. 1, that electron trapping in surface-related defects may initiate electrostatic adsorption of electrolyte cations (ETIEA), and that ETIEA may modify the dynamics of electron transport and consequently lead to the continuous decay of photoactivity. In the following context, experimental supports from two aspects, *i.e.* the occurrence of ETIEA and a continuous decay of electron transport properties during the PEC process will be provided.

### 3.4 Electron trapping induced electrostatic adsorption of electrolyte cations (ETIEA)

Nanostructured TiO<sub>2</sub> electrodes have a strong tendency to trap electrons due to the high chemical capacitance of defect states.<sup>21–23</sup> It is reasonable to suppose that electron trapping makes the TiO<sub>2</sub> films negatively charged and consequently initiates ETIEA. The evidence of ETIEA cannot be given directly from PEC reaction systems because of the complicated dynamic processes of charge carriers in both the semiconductor and electrolyte. Herein, electron trapping is realized by applying negative potentials to TiO<sub>2</sub> electrodes in the dark. Under such a simple system, applied potential  $V_{app}$  (corresponding to the electron Fermi level,  $E_{Fn}$ ) is the only variable to control the population of trap states (Fig. 5a and b). Thus, the influence of electron trapping on the system can be easily detected. In this work, three electron trapping experiments are carried out.

**3.4.1 Electron-trapping induced MB adsorption.** The TiO<sub>2</sub> films are immersed in anaerobic MB solution in a dark PEC cell. Under open circuit conditions, adsorption equilibriums when the amount of adsorbed MB is kept unchanged are reached after *ca.* 600 minutes (Fig. 6). However, more MB molecules are

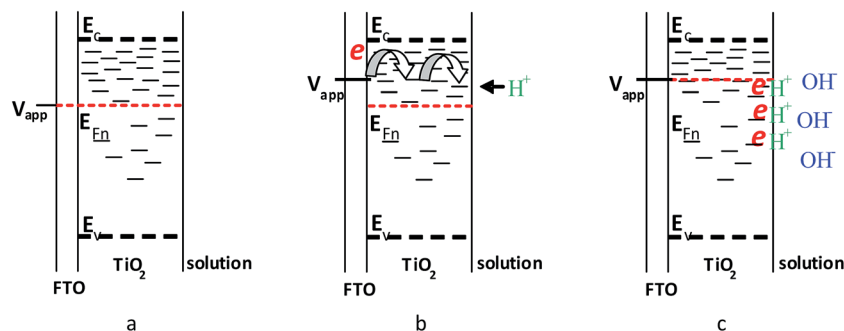


Fig. 5 Schematic illustrations of (a) the FTO|TiO<sub>2</sub>|electrolyte system, (b) electron trapping induced proton (H<sup>+</sup>) and/or other cation adsorption and (c) ETPE induced OH<sup>-</sup> excess in the solution side. The red dashed line marks the  $E_{Fn}$ ; the trap states (short lines) above or below the  $E_{Fn}$  are unpopulated or populated.

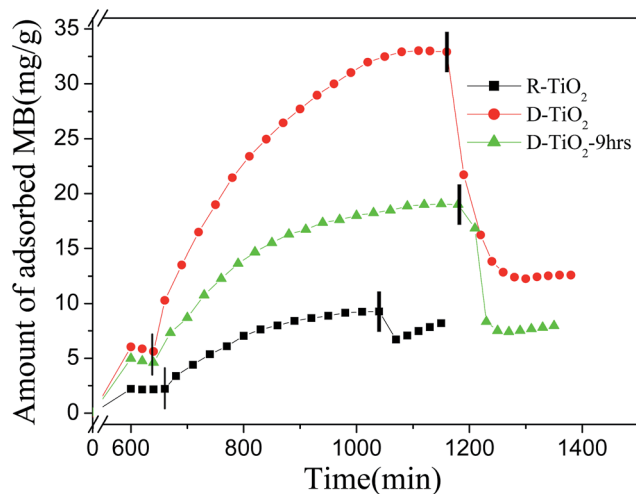


Fig. 6 Time dependent evolution of the amount of adsorbed MB (per unit mass of  $\text{TiO}_2$ ) during the electron trapping experiments. In the range of 0–600 minutes, the system is in the open circuit state. A  $-0.8$  V bias is applied between the thin line and the thick line. After the thick line the bias is shifted to  $0.8$  V.

adsorbed when a  $-0.8$  V bias is applied. It takes another 200–600 minutes (between the thin line and the thick line in Fig. 6) for these films to reach a second equilibrium.

The point of zero charge of  $\text{TiO}_2$  ( $\text{pH}_{\text{PZC}}$ ) is about 5.5, which makes the  $\text{TiO}_2$  surface negatively charged in neutral solution and thus have a tendency to adsorb the cationic dye MB.<sup>14</sup> Under open circuit conditions, the amount of adsorbed MB at equilibrium ( $A_e$ ) is directly related to the EASA of the  $\text{TiO}_2$  films (Fig. 4a), leading to  $A_{e-\text{D-TiO}_2}$  that is quite close to  $A_{e-\text{D-TiO}_2-9\text{h}}$  but much larger than both  $A_{e-\text{R-TiO}_2}$  and  $A_{e-\text{FTO}}$  (Fig. 6 and S10†).

Under the electron-trapping state, however, the  $A_e$  is correlated much more with the total amount of surface defects rather than the EASA of the  $\text{TiO}_2$  films. It can be seen that at  $-0.8$  V bias the  $A_{e-\text{D-TiO}_2-9\text{h}}$  is much smaller than  $A_{e-\text{D-TiO}_2}$  although the EASA of the two films is quite close (Fig. 4a). The same trend has also been observed in the variation of the total amount of surface defects after the long time heat treatment (Fig. 4b). On the other hand, enlargements of  $A_e$  by 4.39–5.69 times for the three films can be reached when the system is shifted from the open circuit to the electron trapping state. Applying a  $0.8$  V bias leads to the release of the adsorbed MB molecules due to the fact that the trapped electrons are extracted out into the external circuit; the amount of desorbed MB also corresponds to the amount of surface defects (Fig. 6). These facts give an important

implication that electron trapping in defect states creates new adsorption sites which show much stronger adsorption capacity for cations. In other words, the ETIEA may be different from common physical adsorption by the much stronger electrostatic interactions of electrons with electrolyte cations.

**3.4.2 Electron-trapping induced proton adsorption (ETPA) in  $\text{KNO}_3$  solution.** For PEC systems where aqueous electrolyte solutions, for example  $1$  M  $\text{KNO}_3$  herein, are used, ETPA as a special case of ETIEA may be dominant considering the smallest diameter, quite strong polarizing power of protons and PEC-induced proton excess around the  $\text{TiO}_2$  film. This viewpoint can be supported by recent reports.<sup>66,69</sup>

In neutral solutions ( $\text{pH} = 7$ ), ETPA may lead to  $\text{OH}^-$  excess at the  $\text{TiO}_2$ /electrolyte interface (see Fig. 5c). However, the pH meter failed to detect such a change, which may indicate that the ETPA-induced  $\text{OH}^-$  excess is established in a very thin layer of solution close to the interface.

Phenolphthalein ( $\text{C}_{20}\text{H}_{14}\text{O}_4$ ) is one of the most commonly used acid–base indicators.<sup>70</sup> The color-changing mechanism is due to the reversible transformation of the molecular structures in different pH environments (Fig. 7). Considering its high sensitivity to pH variation and appropriate color change intervals ( $\text{pH}$  8–10) we select it as the probe to test the ETPA-induced pH change at the  $\text{TiO}_2$ /electrolyte interface.

The pictures in Fig. 8 show the color change of the  $\text{TiO}_2$  electrodes during the electron trapping process. If phenolphthalein is not added into the electrolyte, the color of the film after applying a  $-0.9$  V bias will change from white to light gray due to the light absorption of electrons in the conduction band and trap states of  $\text{TiO}_2$  (Fig. 5a and b).<sup>71,72</sup> On the contrary, the color of the film turns gradually from white to pink if phenolphthalein is added beforehand, indicating a weak base condition is formed (Fig. 8c). Moreover, the pink color can only be detected in the surface of the  $\text{TiO}_2$  film. Therefore, the  $\text{OH}^-$ -excess condition at the interface of  $\text{TiO}_2$ /electrolyte confirms the occurrence of ETPA.

As for the color-changing experiments, another three important issues should be pointed out. Firstly, the EASA comes mainly from the internal surface of the nanoporous framework of the  $\text{TiO}_2$  film (Fig. 3b and S2†); the ETPA-induced  $\text{OH}^-$  excess occurs mainly within the nanopores. Consequently, the diffusion of  $\text{OH}^-$  towards the bulk solution may be hindered, causing a pH rise only within the confined domains. Secondly, even if the electron trapping goes on for a long period of time (500 s) the pink color does not disappear, indicating that ETPA is kinetically stable. At the same time, this also proves that the

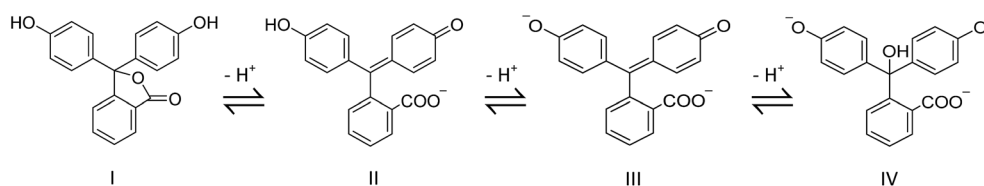


Fig. 7 Schematic illustrations of the phenolphthalein coloration process. In a neutral or weak acid solution, it has a lactone structure (I) which is colorless. In a weak base solution, it loses one or two protons yielding quinone structures (II or III) which show a red color. The quinone structure in a strong base solution will further transform into a colorless methanol-type structure (IV).

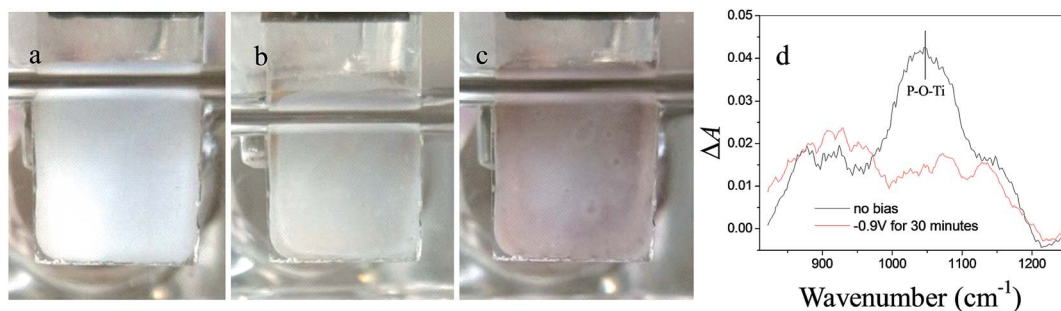


Fig. 8 Pictures of the D-TiO<sub>2</sub> electrode in the PEC cell, (a) before the electron trapping experiment and with phenolphthalein in the electrolyte; (b) during electron trapping and without phenolphthalein in the electrolyte; (c) during electron trapping and with phenolphthalein in the electrolyte. (d) Difference IR spectra of the phosphate-modified TiO<sub>2</sub> to show the dissociation of P–O–Ti bonds after being subjected to the “electron trapping” experiment; the IR spectra after being subjected to electron trapping at –0.9 V for 120 minutes was used as the control (Fig. S11†).

–0.9 V bias cannot initiate the water electrolysis reaction, that is, no OH<sup>–</sup> ions are formed through the reaction  $\text{H}_2\text{O} + \text{e}^- = \text{OH}^- + 1/2\text{H}_2$ . Otherwise, a very high OH<sup>–</sup>-excess condition (strong base condition) will cause phenolphthalein to further transform into a colorless methanol-type structure (IV). Finally, the pink color disappears instantly as long as the applied bias is shifted to +0.6 V (please check the ESI† for video file 1). At this positive bias, the trapped electrons leave TiO<sub>2</sub> and flow back to the external circuit, at the same time the adsorbed protons re-enter the electrolyte solution. As a result, the neutral pH condition at the TiO<sub>2</sub>/interface is regained and the indicator molecules restore the initial colorless lactone structure (I). This color-changing experiment proves that the ETPA is a reversible process and further confirms that the OH<sup>–</sup> excess is not due to the irreversible water electrolysis reaction.

Applying a strong negative bias (usually more negative than –1.4 V vs. Ag/AgCl) to TiO<sub>2</sub> electrodes can initiate electrochemical doping of protons or Li<sup>+</sup>. The intercalated protons/Li<sup>+</sup> can effectively deactivate the traps and lead to the well known “trap-filling” effect which remarkably improves the conductivity of TiO<sub>2</sub>.<sup>26,29–32,73</sup> While, the ETPA may not initiate the “trap-filling” effect, as the energy levels of these band gap states are too low. Therefore, the nature of ETPA should be of electrostatic interaction (like that of MB adsorption shown in Fig. 6), which endows ETPA with a reversible character. The instant

disappearance of the red color when a positive bias is applied (less than one second and displayed in video file 1 in the ESI†) implies that most protons are probably not inserted into the TiO<sub>2</sub> lattice but adsorbed electrostatically on the TiO<sub>2</sub> surface. The same situation can also be seen in Fig. 6 which shows that the dye molecules are desorbed quickly when trapped electrons are extracted out. On the contrary, spectrometry and electrochemical investigations indicate that the inserted protons or Li<sup>+</sup> in the TiO<sub>2</sub> lattice are relatively stable,<sup>26,74–77</sup> and the decay of open circuit photovoltage ( $V_{oc}$ ) demonstrated that the release of the inserted Li<sup>+</sup> can proceed over thousands of seconds.<sup>26</sup> The color-changing experiment was also carried out to track proton insertion (at –1.4 V) and release (at 0.6 V) processes, indicating that the release of the inserted protons can proceed for more than three minutes (video file 2 in the ESI†). Therefore, the adsorbed cations such as protons and MB should be mainly located at the surface defect and/or grain boundary defect sites where electrons are simultaneously trapped, which has been described as the origin of “shallow” energy localized states associated with Ti<sup>3+</sup> in the lattice.<sup>71,78</sup>

It is well known that phosphate groups can be chemically adsorbed to the TiO<sub>2</sub> surface through covalent Ti–O–P connections which show characteristic absorptions centered at ca. 1050 cm<sup>–1</sup> in IR spectra (Fig. 8d and S11†).<sup>14,37,79</sup> It has been proven that the hydrolysis of Ti–O–P connections can only occur

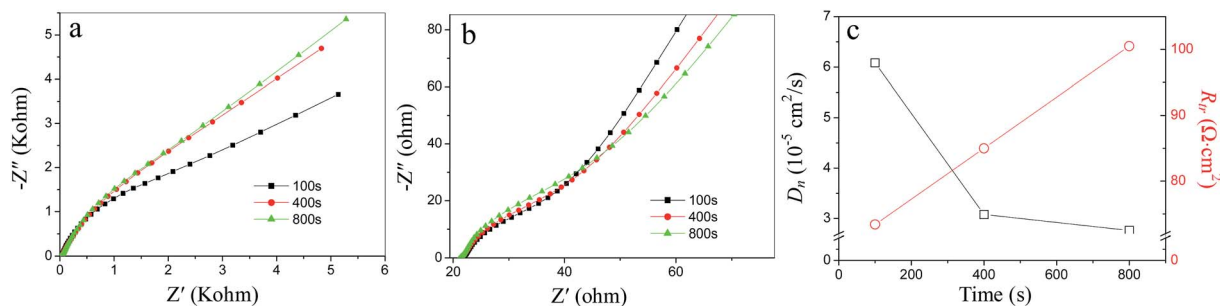


Fig. 9 (a) The Nyquist plots of the D-TiO<sub>2</sub> film from a series of combined  $i-t$  and EIS measurements; (b) the enlarged part of (a) in high frequency domain, inset is the time of the  $i-t$  processes. (c) The evolutions of  $D_n$  and  $R_{tr}$  along with the proceeding of the  $i-t$  processes. The direct bias for the EIS measurements is –0.16 V.

in alkaline solutions but not in neutral or acidic solutions.<sup>80</sup> The IR spectra indicate the dissociation of the covalent Ti–O–P connections after the electron trapping experiment, further confirming the occurrence of the ETPE process (Fig. 8d).

### 3.5 Continuous decay of electron transport properties during the *i*-*t* process

The above electron trapping experiments indicate that the interactions between trapped electrons and electrolyte cations are general and even dominant when the amount of surface defects increases to some extent as in D-TiO<sub>2</sub>. Meanwhile, the reversible character of the ETIEA implies that the nature of these interactions should still be of weak electrostatic interactions, which can be destroyed by thermal energy *KT*. This means that this interaction should not be strong enough to passivate traps permanently, that is, to cause the well known “trap-filling” effect.<sup>26–32</sup> Therefore, it is reasonable to suppose that the ETIEA may play a role in slowing down electron transport during various photo/electrochemical processes.

Two combined photo/electrochemical measurement techniques, that is, *i*-*t*/potential-step chronoamperometry (PSCA) (S3†) and *i*-*t*/electrochemical impedance (EIS) (S4†) are developed to explore the evolution of electron transport properties during the *i*-*t* process. Fig. 9a and b show the Nyquist plots of the same D-TiO<sub>2</sub> electrode which change along with the proceeding of the *i*-*t* processes. The electron diffusion coefficient (*D*<sub>n</sub>) can be further calculated by using eqn (1) where *l*, *C*<sub>μ</sub>, and *R*<sub>tr</sub> are respectively film thickness, chemical capacitance and electron transport resistance.<sup>34,51</sup> Fig. 9c, s12b and d† indicate that during the initial stage (at least the first 10 minutes demonstrated herein) prolonging the PEC process will continuously deteriorate electron transport properties.

As far as electron mobility does not change, *R*<sub>tr</sub> only varies with the Fermi level (electron density) for a given system of nanostructured semiconductor/electrolyte in the dark.<sup>21,23</sup> However, the current research suggests that along with the proceeding of the *i*-*t* process electron mobility can change continuously because the Fermi level is kept unchanged while *R*<sub>tr</sub> varies. The lattice scattering effect due to structural disorder and the “trapping–detrapping” dynamics are two main factors responsible for the low electron mobility of nanostructured semiconductors.<sup>25</sup> For a given film as in Fig. 9, s12 and s14,† apparently, the former will be kept unchanged while the latter can be altered as the trap states may be modified during the PEC process. As proposed in Fig. 1, the electrostatic attractions between trapped electrons and cations (protons and/or other cations in the electrolyte) will increase the energy barrier of detrapping, resulting in a continuous decay of electron transport properties.

$$D_n = \frac{l^2}{C_\mu \times R_{tr}} \quad (1)$$

It should be pointed out that the influence of electrolyte on electron dynamics has been studied at least 16 years ago.<sup>68</sup> Electron transport in an electrolyte-filled mesoporous TiO<sub>2</sub> network is described as “ambipolar diffusion”.<sup>64</sup> In this model,

the motion of electrons causes a charge imbalance and the resulting electric field will drag the cations along with them. As a result, electron transport is retarded since the diffusion of electrons in the semiconductor has a different speed from that of cations in the electrolyte. This mode gave a new diffusion coefficient *D*<sub>amb</sub> to differentiate from the pure diffusion behavior of electrons (eqn (2)).

$$D_{amb} = \frac{n + p}{n/D_p + p/D_n} \quad (2)$$

where *D*<sub>p</sub> and *D*<sub>n</sub> represent the diffusion coefficient of ions and electrons and *p* and *n* are the respective densities of ions and electrons. However, eqn (2) suggests that the *D*<sub>amb</sub> is, to a good approximation, the same as *D*<sub>n</sub> in the common photo/electrochemical systems (*D*<sub>amb</sub> = *D*<sub>n</sub>) because the electron concentration (<10<sup>18</sup> cm<sup>-3</sup>) in TiO<sub>2</sub> films is generally much less than the ion concentration (in the order of 10<sup>21</sup> cm<sup>-3</sup> corresponding to ~1 M monovalent ions).<sup>64,68</sup> This means that the actual influence of electrolyte on electron diffusion can be neglected. Apparently, the continuous decay of the electron transport behavior shown in Fig. 9 and S3† is not compatible with the ambipolar diffusion mode, which is probably due to the fact that this mode does not include surface trap involved interactions between electrons and electrolyte cations.<sup>81</sup>

### 3.6 ETIEA induced photoactivity decay

This work indicates that ETIEA may be general for some nanostructured TiO<sub>2</sub> electrodes used in photo/electrochemical systems. Along with the proceeding of ETIEA, more and more trapped electrons have an enlarged energy barrier for detrapping due to the electrostatic interactions, leading to a continuous increase of transport resistance especially during the first 10 minutes of the *i*-*t* process herein. Thus, ETIEA is considered as the essential cause of the general and continuous photoactivity decay typically shown in Fig. 2.

As for the ETIEA-induced photoactivity decay, the surface defects play a key role. It is reasonable to consider that more surface defects correspond to much larger ETIEA and consequently result in much faster photoactivity decay. Our measurements have given some evidence. The three films R-TiO<sub>2</sub>, D-TiO<sub>2</sub> and D-TiO<sub>2</sub>-9 h are made with the same mass of TiO<sub>2</sub> and geometric electrode area, while the R-TiO<sub>2</sub> film has the least amount of surface defects (Fig. 4b and 6) and the slowest decay (Fig. 2b). The 9 hour heat treatment on the D-TiO<sub>2</sub> film changes little the EASA (Fig. 4a) but reduces remarkably surface defects (Fig. 4b); correspondingly, the decay is slowed down (Fig. s7†). Therefore, it is the total amount of surface defects that is directly related to the rate of photoactivity decay.

It should be pointed out that the factors related to the photoactivity decay of nanostructured electrodes should be multiple. Based on the unusual ion diffusion in nano-dimensional channels<sup>82,83</sup> and ETIEA, we are now trying to explain the influence of electrolyte concentration on photoactivity decays which is demonstrated in Fig. s3f–h.†

The existence of surface defect states is inevitable for nanostructured inorganic semiconductors, which is why R-TiO<sub>2</sub> still

shows slow photocurrent decay despite its single crystal nature. Moreover, proton charge compensation uptake is also common for many other metal oxides.<sup>84</sup> The above factors make us further propose that the negative influence of ETPA on photoactivity should be general in various non-TiO<sub>2</sub> PEC systems, which needs to be confirmed with more experimental evidence.

## 4. Conclusion

This work displayed a continuous and reversible photocurrent decay which is general for nanostructured TiO<sub>2</sub> photoelectrodes. During the proceeding of the photo/electrochemical process electrons are trapped in surface defect states, leading to electrostatic adsorption of protons and other cations from the electrolyte. The electrostatic interactions undermine electron transport properties probably by increasing the energy barrier for electron detrapping, which consequently leads to a continuous photocurrent decay during the initial several minutes of the PEC process.

## Acknowledgements

This work was supported by the NSFC (Grant No. 21171144, 21671205, and 21502134), the NSF of Shandong province (Grant No. ZR2013EMQ004 and J13LD11), the Basic and Frontier Technical Research Project of Henan Province (Grant No. 152300410228) and the University Innovation Team Project in Henan Province (Grant No. 15IRTSTHN004), China.

## References

- 1 M. Grätzel, *J. Photochem. Photobiol., C*, 2003, **4**, 145–153.
- 2 M. R. Hoffmann, S. T. Martin, W. Y. Choi and D. W. Bahnemann, *Chem. Rev.*, 1995, **95**, 69–96.
- 3 A. L. Linsebigler, G. Q. Lu and J. T. Yates, *Chem. Rev.*, 1995, **95**, 735–758.
- 4 R. Dagherir, P. Drogui and D. Robert, *Ind. Eng. Chem. Res.*, 2013, **52**, 3581–3599.
- 5 T. Ochiaiaia and A. Fujishima, *J. Photochem. Photobiol., C*, 2012, **13**, 247–262.
- 6 A. Fujishima and K. Honda, *Nature*, 1972, **238**, 37–38.
- 7 F. E. Osterloh, *Chem. Soc. Rev.*, 2013, **42**, 2294–2320.
- 8 J. R. Swierka and T. E. Mallouk, *Chem. Soc. Rev.*, 2013, **42**, 2357–2387.
- 9 H. D. Jang, S. K. Kim, H. Chang, K. Roh, J. Choi and J. Huang, *Biosens. Bioelectron.*, 2012, **38**, 184–188.
- 10 H. Dai, S. Zhang, Z. Hong, X. Li, G. Xu, Y. Lin and G. Chen, *Anal. Chem.*, 2014, **86**, 6418–6424.
- 11 D. Monllor-Satoca and R. Gómez, *Electrochim. Acta*, 2010, **55**, 4661–4668.
- 12 J. Yu and B. Wang, *Appl. Catal., B*, 2010, **94**, 295–302.
- 13 A. Hagfeldt, H. Lindström, S. Södergren and S. E. Lindquist, *J. Electroanal. Chem.*, 1995, **381**, 39–46.
- 14 T. He, Y. G. Weng, P. Yu, C. L. Liu, H. Q. Lu, Y. P. Sun, S. Z. Zhang, X. Yang and G. Q. Liu, *J. Phys. Chem. C*, 2014, **118**, 4607–4617.
- 15 T. Berger, D. Monllor-Satoca, M. Jankulovska, T. Lana-Villarreal and R. Gómez, *ChemPhysChem*, 2012, **13**, 2824–2875.
- 16 A. J. Bard, A. B. Bocarsly, F. F. Fan, E. G. Walton and M. S. Wrighton, *J. Am. Chem. Soc.*, 1980, **102**, 3671–3677.
- 17 K. Sivula, *J. Phys. Chem. Lett.*, 2013, **4**, 1624–1633.
- 18 J. E. Thorne, S. Li, C. Du, G. Qin and D. Wang, *J. Phys. Chem. Lett.*, 2015, **6**, 4083–4088.
- 19 F. L. Formal, S. R. Pendlebury, M. Cornuz, S. D. Tilley, M. Grätzel and J. R. Durrant, *J. Am. Chem. Soc.*, 2014, **136**, 2564–2574.
- 20 B. Klahr, S. Gimenez, F. Fabregat-Santiago, T. Hamann and J. Bisquert, *J. Am. Chem. Soc.*, 2012, **134**, 4294–4302.
- 21 J. Bisquert, *Phys. Chem. Chem. Phys.*, 2003, **5**, 5360–5364.
- 22 M. Jankulovska, T. Berger, S. S. Wong, R. Gómez and T. Lana-Villarreal, *ChemPhysChem*, 2012, **13**, 3008–3017.
- 23 F. Fabregat-Santiago, I. Mora-Seró, G. Garcia-Belmonte and J. Bisquert, *J. Phys. Chem. B*, 2003, **107**, 758–768.
- 24 J. Villanueva-Cab, S. R. Jang, A. F. Halverson, K. Zhu and A. J. Frank, *Nano Lett.*, 2014, **14**, 2305–2309.
- 25 P. E. De Jongh and D. Vanmaekelbergh, *Phys. Rev. Lett.*, 1996, **77**, 3427–3430.
- 26 B. H. Meekins and P. V. Kamat, *ACS Nano*, 2009, **3**, 3437–3446.
- 27 G. M. Wang, Y. Yang, Y. C. Ling, H. Y. Wang, X. H. Lu, Y. C. Pu, J. Z. Zhang, Y. X. Tong and Y. Li, *J. Mater. Chem. A*, 2016, **4**, 2849–2855.
- 28 J. Zhao, E. Olide and F. E. Osterloh, *J. Electrochem. Soc.*, 2015, **162**, H65–H71.
- 29 F. Fabregat-Santiago, E. M. Barea, J. Bisquert, G. K. Mor, K. Shankar and C. Grimes, *J. Am. Chem. Soc.*, 2008, **130**, 11312–11316.
- 30 J. Idigoras, T. Berger and J. A. Anta, *J. Phys. Chem. C*, 2013, **117**, 1561–1570.
- 31 K. Schwarzburg and F. Willig, *Appl. Phys. Lett.*, 1991, **58**, 2520–2522.
- 32 X. H. Lu, G. M. Wang, T. Zhai, M. H. Yu, J. Y. Gan, Y. X. Tong and Y. Li, *Nano Lett.*, 2012, **12**, 1690–1696.
- 33 N. Kopidakis, K. D. Benkstein, J. van de Lagemaat and A. J. Frank, *Phys. Rev. B: Condens. Matter Mater. Phys.*, 2006, **73**, 045326.
- 34 J. Bisquert and V. S. Vikhrenko, *J. Phys. Chem. B*, 2004, **108**, 2313–2322.
- 35 J. Nelson, S. A. Haque, D. R. Klug and J. R. Durrant, *Phys. Rev. B: Condens. Matter Mater. Phys.*, 2001, **63**, 797–801.
- 36 B. Liu and E. S. Aydil, *J. Am. Chem. Soc.*, 2009, **131**, 3985–3990.
- 37 J. C. Yu, L. Z. Zhang, Z. Zheng and J. C. Zhao, *Chem. Mater.*, 2003, **15**, 2280–2286.
- 38 P. Basnet and Y. Zhao, *Catal. Sci. Technol.*, 2015, **6**, 2228–2238.
- 39 A. Paracchino, V. Laporte, K. Sivula, M. Grätzel and E. Thimsen, *Nat. Mater.*, 2011, **10**, 456–461.
- 40 Q. Huang, F. Kang, H. Liu, Q. Li and X. Xiao, *J. Mater. Chem. A*, 2013, **1**, 2418–2425.
- 41 D. Kang, T. W. Kim, S. R. Kubota, A. C. Cardiel, H. G. Cha and K. Choi, *Chem. Rev.*, 2015, **115**, 12839–12887.

- 42 R. van de Krol and M. Grätzel, *Photoelectrochemical hydrogen production*, Springer, New York, Dordrecht, Heidelberg, London, 1st edn, 2012.
- 43 T. Walter, R. Herberholz, C. Müller and H. W. Schock, *J. Appl. Phys.*, 1996, **80**, 4411–4420.
- 44 M. S. Faber, R. Dziedzic, M. A. Lukowski, N. S. Kaiser, Q. Ding and S. Jin, *J. Am. Chem. Soc.*, 2014, **136**, 10053–10061.
- 45 H. Liang, F. Meng, M. Caban-Acevedo, L. Li, A. Forticaux, L. Xiu, Z. Wang and S. Jin, *Nano Lett.*, 2015, **15**, 1421–1427.
- 46 M. Grätzel and A. J. Frank, *J. Phys. Chem.*, 1982, **86**, 2964–2967.
- 47 M. Lv, D. Zheng, M. Ye, L. Sun, J. Xiao, W. Guo and C. Lin, *Nanoscale*, 2012, **4**, 5872–5879.
- 48 J. Procházka, L. Kavan, V. Shklover, M. Zukalová, O. Frank, M. Kalbáč, A. Zukal, H. Pelouchová, P. Janda, K. Mocek, M. Klementová and D. Carbone, *Chem. Mater.*, 2008, **20**, 2985–2993.
- 49 B. O'Regan and M. Grätzel, *Nature*, 1991, **353**, 737–740.
- 50 T. Berger, T. Lana-Villarreal, D. Monllor-Satoca and R. Gómez, *J. Phys. Chem. C*, 2007, **111**, 9936–9942.
- 51 Q. Wang, S. Ito, M. Grätzel, F. Fabregat-Santiago, I. Mora-Seró, J. Bisquert, T. Bessho and H. Ima, *J. Phys. Chem. B*, 2006, **110**, 25210–25221.
- 52 G. Yang, R. A. C. M. M. van Swaaij, S. Dobrovolskiy and M. Zeman, *J. Appl. Phys.*, 2014, **115**, 034512.
- 53 H. Wang, J. He, G. Boschloo, H. Lindstrom, A. Hagfeldt and S. Lindquist, *J. Phys. Chem. B*, 2001, **105**, 2529–2533.
- 54 N. Kopidakis, N. R. Neale, K. Zhu, J. van de Lagemaat and A. J. Frank, *Appl. Phys. Lett.*, 2005, **87**, 202106.
- 55 F. Nunzi, E. Mosconi, L. Storch, E. Ronca, A. Selloni, M. Grätzel and F. De Angelis, *Energy Environ. Sci.*, 2013, **6**, 1221–1229.
- 56 Q. Zhang, V. Celorrio, K. Bradley, F. Eisner, D. Cherns, W. Yan and D. Fermín, *J. Phys. Chem. C*, 2014, **118**, 18207–18213.
- 57 G. Boschloo and D. Fitzmaurice, *J. Phys. Chem. B*, 1999, **103**, 2228–2231.
- 58 A. Kudo and Y. Miseki, *Chem. Soc. Rev.*, 2009, **38**, 253–278.
- 59 J. Chen, H. B. Yang, J. Miao, H. Wang and B. Liu, *J. Am. Chem. Soc.*, 2014, **136**, 15310–15318.
- 60 S. H. Kang, S. Choi, M. Kang, J. Kim, H. Kim, T. Hyeon and Y. Sung, *Adv. Mater.*, 2008, **20**, 54–58.
- 61 M. Kong, Y. Li, X. Chen, T. Tian, P. Fang, F. Zheng and X. Zhao, *J. Am. Chem. Soc.*, 2011, **133**, 16414–16417.
- 62 J. Yan, G. Wu, N. Guan, L. Li, Z. Li and X. Cao, *Phys. Chem. Chem. Phys.*, 2013, **15**, 10978–10988.
- 63 J. Bisquert, *J. Phys. Chem. C*, 2007, **111**, 17163–17168.
- 64 A. J. Frank, N. Kopidakis and J. van de Lagemaat, *Coord. Chem. Rev.*, 2004, **248**, 1165–1179.
- 65 J. Zhang, M. Steigerwald, L. Brus and R. A. Friesner, *Nano Lett.*, 2014, **14**, 1785–1789.
- 66 A. F. Halverson, K. Zhu, P. T. Erslev, J. Y. Kim, N. R. Neale and A. J. Frank, *Nano Lett.*, 2012, **12**, 2112–2116.
- 67 W. Yang, M. Pazoki, A. Eriksson, Y. Hao and G. Boschloo, *Phys. Chem. Chem. Phys.*, 2015, **17**, 16744–16751.
- 68 N. Kopidakis, E. A. Schiff, N. Park, J. van de Lagemaat and A. J. Frank, *J. Phys. Chem. B*, 2000, **104**, 3930–3936.
- 69 J. R. Swierk, N. S. McCool, T. P. Saunders, G. D. Barber and T. E. Mallouk, *J. Am. Chem. Soc.*, 2014, **136**, 10974–10982.
- 70 C. A. Peters and B. C. Redmon, *J. Chem. Educ.*, 1940, **17**, 525–528.
- 71 G. Boschloo and D. Fitzmaurice, *J. Phys. Chem. B*, 1999, **103**, 7860–7868.
- 72 B. O'Regan, M. Grätzel and D. Fitzmaurice, *Chem. Phys. Lett.*, 1991, **183**, 89–93.
- 73 Q. Wang, Z. Zhang, S. M. Zakeeruddin and M. Grätzel, *J. Phys. Chem. C*, 2008, **112**, 7084–7092.
- 74 D. Bahnemann, A. Henglein, J. Lilie and L. Spanhel, *J. Phys. Chem.*, 1984, **88**, 709–711.
- 75 R. F. Howe and M. Grätzel, *J. Phys. Chem.*, 1985, **89**, 4495–4499.
- 76 N. Serpone, D. Lawless, R. Khairutdinov and E. Pelizzetti, *J. Phys. Chem.*, 1995, **99**, 16655–16661.
- 77 K. Vinodgopal, X. Hua, R. Dahlgren, A. G. Lappin, L. K. Patterson and P. V. Kamat, *J. Phys. Chem.*, 1995, **99**, 10883–10889.
- 78 H. Lindström, S. Södergren, A. Solbrand, H. Rensmo, J. Hjelm, A. Hagfeldt and S. E. Lindquist, *J. Phys. Chem. B*, 1997, **101**, 7717–7722.
- 79 L. Körösi, S. Papp, I. Bertóti and I. Dékány, *Chem. Mater.*, 2007, **19**, 4811–4819.
- 80 K. Hadjiivanov, D. Klissurski and A. Davydov, *J. Catal.*, 1989, **116**, 498–505.
- 81 D. Nistér, K. Keis, S. Lindquist and A. Hagfeldt, *Sol. Energy Mater. Sol. Cells*, 2002, **73**, 411–423.
- 82 Q. Pu, J. Yun, H. Temkin and S. Liu, *Nano Lett.*, 2004, **4**, 1099–1103.
- 83 M. van Soestbergen, *Electrochem. Commun.*, 2012, **20**, 105–108.
- 84 B. I. Lemon and J. T. Hupp, *J. Phys. Chem. B*, 1997, **101**, 2426–2429.